THE JOURNAL OF BIOLOGICAL CHEMISTRY VOL. 284, NO. 43, pp. 29956–29967, October 23, 2009

Acetylation of Transition Protein 2 (TP2) by KAT3B (p300) Alters Its DNA Condensation Property and Interaction with Putative Histone Chaperone NPM3*

Received for publication, August 4, 2009, and in revised form, August 25, 2009 Published, JBC Papers in Press, August 26, 2009, DOI 10.1074/jbc.M109.052043

Madapura M. Pradeepa[‡1], Gupta Nikhil[‡1], Annavarapu Hari Kishore[‡], Giriyapura N. Bharath[‡], Tapas K. Kundu[‡], and Manchanahalli R. Satyanarayana Rao[‡§2]

From the [‡]Molecular Biology and Genetics Unit, Jawaharlal Nehru Centre for Advanced Scientific Research, Jakkur P. O., Bangalore 560064, India and the [§]Department of Biochemistry, Indian Institute of Science, Bangalore 560012, India

The hallmark of mammalian spermiogenesis is the dramatic chromatin remodeling process wherein the nucleosomal histones are replaced by the transition proteins TP1, TP2, and TP4. Subsequently these transition proteins are replaced by the protamines P1 and P2. Hyperacetylation of histone H4 is linked to their replacement by transition proteins. Here we report that TP2 is acetylated *in vivo* as detected by anti-acetylated lysine antibody and mass spectrometric analysis. Further, recombinant TP2 is acetylated *in vitro* by acetyltransferase KAT3B (p300) more efficiently than by KAT2B (PCAF). *In vivo* p300 was demonstrated to acetylate TP2. p300 acetylates TP2 in its C-terminal domain, which is highly basic in nature and possesses chromatin-condensing properties. Mass spectrometric analysis showed that p300 acetylates four lysine residues in the C-terminal domain of TP2. Acetylation of TP2 by p300 leads to significant reduction in its DNA condensation property as studied by circular dichroism and atomic force microscopy analysis. TP2 also interacts with a putative histone chaperone, NPM3, wherein expression is elevated in haploid spermatids. Interestingly, acetylation of TP2 impedes its interaction with NPM3. Thus, acetylation of TP2 adds a new dimension to its role in the dynamic reorganization of chromatin during mammalian spermiogenesis.

The process of spermiogenesis in mammals, wherein the haploid round spermatids mature into highly condensed spermatozoa, can be divided broadly into three phases. In the first phase, which encompasses stages 1–10, the round spermatids are transcriptionally active and contain nucleosomal chromatin. The second phase (stages 12–15) involves the replacement of nucleosomal histones by transition proteins TP1, TP2, and TP4. These transition proteins, localized exclusively to the nuclei of elongating and condensing spermatids (1), constitute about 90% of the chromatin basic proteins, with the level of TP1 being about 2.5 times those of TP2 (2). Finally, in the third phase, the transition proteins are replaced by protamines P1 and P2 during stages 16–19 (1, 3). The biological significance of the evolution of transition protein genes and their physiological roles are not yet completely understood. Both $TP1^{-/-}$ and $TP2^{-/-}$ knock-out mice have been generated; they are less fertile than normal mice and show abnormal chromatin condensation (2, 4). TP1 and TP2 double knock-out mice are, however, sterile, and spermatogenesis is severely impaired suggesting their important and essential role in spermiogenesis (5). Although the individual function of transition proteins (TPs)[3] remains unclear, TP1 and TP2 do not fully compensate for one another, and each likely fulfils certain unique roles (6).

TP2 is a basic protein of molecular mass of 13 kDa possessing DNA and chromatin condensation properties (7, 8). TP2 is a zinc metalloprotein and contains two atoms of zinc per molecule (9); it condenses DNA with a preference for GC-rich DNA in a zinc-dependent manner (10). The domain architecture of TP2 has been delineated and shown to possess two structural and functional domains, the zinc finger modules coordinating the two zinc atoms in TP2 in the N terminus (11) and the C-terminal basic domain. Immediately after synthesis, TP2 becomes phosphorylated in the cytosol by the sperm-specific isoform of the catalytic subunit of protein kinase A (Cs-PKA) (12) and modulates the nuclear import of TP2 (13). Recently, a nuclear localization signal of TP2 was shown to interact with importin-4, which mediates the transport of TP2 into the spermatid nucleus (14). We had proposed a model depicting the sequence of events leading to TP2 deposition on chromatin and initiation of condensation (12). In this model we had visualized the phosphorylation of TP2 as temporarily inhibiting the condensation property of TP2, allowing lateral diffusion of TP2 along chromatin to facilitate the recognition of GC-rich CpG island sequences by the two zinc finger modules of TP2. A subsequent dephosphorylation triggers the initiation of chromatin condensation by its basic C-terminal domain.

Another major posttranslational modification of histones and non-histone nuclear proteins is acetylation. Reversible

* This work was supported by grants from the Department of Biotechnology, Ministry of Science and Technology, New Delhi, India.

[1] Supported by a fellowship from the Council of Scientific and Industrial Research, New Delhi, India.

[2] Supported by the J. C. Bose Fellowship from the Department of Science and Technology, Ministry of Science and Technology. To whom correspondence should be addressed: Molecular Biology and Genetics Unit, Jawaharlal Nehru Centre for Advanced Scientific Research, Jakkur P. O., Bangalore 560064, India. Tel.: 91-80-2208-2864; Fax: 91-80-2362-2762; E-mail: mrsrao@jncasr.ac.in.

[3] The abbreviations used are: TP, transition protein; KAT, lysine acetyltransferase; CBP, CREB-binding protein; CREB, cAMP-response element-binding protein; PCAF, p300/CBP-associated factor; NAP1, nucleosome assembly protein 1; MALDI-TOF, matrix-assisted laser desorption/ionization time of flight; NPM, nucleoplasmin; AFM, atomic force microscopy; GST, glutathione *S*-transferase; PBS, phosphate-buffered saline; DAPI, 4,6-diamidino-2-phenylindole; Ac-K, acetylated lysine.

acetylation of nuclear proteins plays a pivotal role in various DNA templated functions such as transcription, replication, and recombination repair in eukaryotic cells (15, 16). At present, more than 30 proteins have been shown to possess acetyltransferase activity, each of which possesses unique substrate specificity. Many of the chromatin-modifying acetyltransferases were initially found to target histone proteins as substrates but were subsequently shown to target non-histone proteins as well, which includes transcription factors, importins, chaperones, chromatin-associated proteins, and cytoskeleton proteins (reviewed in Ref. 17). The acetylation/deacetylation cycle is also associated with several cellular processes independent of transcription, such as protein stability, protein-protein interaction, subcellular localization, and regulation of enzyme activity (reviewed in Ref. 17).

Histones are known to become hyperacetylated in the elongating spermatids, which are functionally associated with their replacement by transition proteins in mammals (18). Histone H4 hyperacetylation coincides with the specific inhibition of deacetylase activity in the elongating spermatids (19). In this context, we were curious to examine whether the transition proteins also undergo acetylation. In this communication, we have been able to detect acetylated TP2 in elongating spermatids. Subsequently, we have found that recombinant TP2 is acetylated *in vitro* by KAT3B (p300) at four lysine residues in its C terminus. Interestingly, we observed that acetylation of TP2 reduces its DNA condensation ability, modulating its interaction with a putative histone chaperone, NPM3.

MATERIALS AND METHODS

All fine chemicals used were purchased from Sigma-Aldrich and Invitrogen. Other general chemicals were obtained from Ranbaxy Chemicals, Qualigens Fine Chemicals, and Merck. Synthetic oligonucleotides used were procured from Sigma. Anti-glutathione *S*-transferase (rabbit polyclonal) and anti-PCAF (rabbit polyclonal) antibodies were obtained from Sigma. Anti-NPM3 (goat polyclonal) and p300 (monoclonal and polyclonal) antibodies were obtained from Santa Cruz Biotechnology. Anti-acetylated lysine antibody (rabbit polyclonal and mouse monoclonal) were obtained from Upstate Biotechnology Inc. and Cell Signaling, respectively. Anti-NPM1 (mouse monoclonal) antibody was obtained from Invitrogen. TP2 antibody was raised in male New Zealand White rabbits using recombinant protein. Secondary antibodies conjugated with Alexa Fluor 488 and 568 dyes were purchased from Molecular Probes. Core histones were isolated from HeLa cell pellet as described previously (20). [^{3}H]Acetyl coenzyme A was obtained from PerkinElmer Life Sciences. TP2 N-terminal (amino acids 11–40) peptides and the middle (amino acids 57–86) and C-terminal (amino acids 85–114) peptides conjugated with biotin were synthesized at Bio-Concept Laboratories. Male Wistar rats were obtained from the animal facility at the Jawaharlal Nehru Centre for Advanced Scientific Research, Bangalore, India. All procedures for handling animals were approved by the animal ethics committee of the Centre.

Cloning, Protein Expression, and Purification—Rat TP2 was expressed and purified as described previously (11). His_6-tagged nucleosome assembly protein 1 (NAP1) was purified with nickel-nitrilotriacetic acid (Qiagen). FLAG epitope-tagged full-length PCAF/KAT2B and His_6-tagged full-length p300/KAT3B were expressed and purified by infection of Sf21 cells with recombinant baculoviruses followed by affinity chromatography of whole-cell extracts on M2-agarose and a nickel-nitrilotriacetic acid column as described elsewhere (21, 22). Native TP2 was purified from sonication-resistant nuclei of adult rat testis by acid extraction and 5–25% trichloroacetic acid precipitation (23) followed by electrophoresis on 15% acid urea PAGE. The TP2 band was excised and electroeluted using 5% acetic acid as the running buffer. Authenticity of the protein was confirmed by trypsin digestion followed by MALDI-TOF analysis. Rat nucleoplasmin 3 (NPM3) (GenBank™ accession number XM_001058548) was amplified by reverse transcription-PCR, cloned into the BamHI and XhoI sites of pGEX4T1, and expressed in BL21 Rosetta cells. The glutathione *S*-transferase (GST) fusion protein was purified using a glutathione-agarose column. Human NPM1 was expressed and purified as described previously (24).

In Vitro Acetylation Reaction—*In vitro* acetylation assays were performed as described elsewhere (20). The indicated amounts of proteins (see the legend to Fig. 2) were incubated at 30 °C for 30 min in a 30-μl final reaction volume consisting of 50 mM Tris-HCl, pH 8.0, 10% (v/v) glycerol, 1 mM dithiothreitol, 1 mM phenylmethylsulfonyl fluoride, 0.1 mM EDTA, pH 8.0, 10 mM sodium butyrate, 0.5 μl of [^{3}H]acetyl coenzyme A (3.3 Ci/mmol) (PerkinElmer Life Sciences), and the respective acetyltransferase enzymes. The reaction mixture was then blotted onto P-81 filter paper. After washing with 0.2 M sodium carbonate buffer, pH 9.2, radioactive counts were recorded in a Wallac 1409 liquid scintillation counter. To visualize the radiolabeled acetylated protein, the reaction products were precipitated with 25% trichloroacetic acid, washed with ice-cold acetone, resolved electrophoretically on a 15% SDS-polyacrylamide gel, and subjected to fluorography using a solution containing 22.5% 2,5-diphenyloxazole in DMSO. Gels were dried, and autoradiography was performed at −80 °C for 2–3 days. Core histones isolated from HeLa cells were used as a positive control, and mouse NAP1 was used as a negative control.

Three microgram of *in vitro* acetylated TP2 (as described earlier) was digested with V8 protease (from *Staphylococcus aureus*, Sigma) in 50 mM ammonium bicarbonate, pH 7.8, at 37 °C for 8 h at an enzyme to protein ratio of 1:50, and the products were separated on 15% acid urea PAGE. The gel was dried, and autoradiography was performed at −80 °C for 2–3 days.

Immunoprecipitation-Acetylation Assay—p300 was immunoprecipitated using anti-p300 monoclonal antibody (Santa Cruz Biotechnology) from postmeiotic haploid cells (purified by centrifugal elutriation) nuclear extract. Bound proteins were resolved on 6% SDS-PAGE, transferred onto nitrocellulose membrane, and probed with anti-p300 polyclonal antibody (Santa Cruz Biotechnology) to detect immunoprecipitated p300 protein. Immuno-pulldown with preimmune serum served as a control. Immunoprecipitated beads were used as enzyme source for acetylation of TP2 and core histones. Acetylation reaction was performed as described above, and the

immunoprecipitate using irrelevant monoclonal antibody served as a negative control. Duplicate samples of core histones were run on a 15% SDS-PAGE and stained with Coomassie Blue.

Immunoblotting and Localization Studies—TP2 purified from rat testis along with recombinant TP2 and core histones isolated from 0–5% trichloroacetic acid precipitates of the acid extract of sonication resistant nuclei were separated in 12% SDS-PAGE, blotted onto nitrocellulose membrane, and probed with antibody against acetylated lysine (Upstate Biotechnology) and TP2. Nuclear extract was prepared from total testicular cells and sonication-resistant spermatids. The protein was quantified, and equal amounts were resolved in SDS-PAGE, blotted onto nitrocellulose, and probed with antibody against NPM1 (Invitrogen), NPM3 (Santa Cruz Biotechnology), and PCAF (Sigma). Duplicate samples were run in SDS-PAGE, one for staining with Coomassie blue and the other for Western blotting.

For indirect immunofluorescence analysis we followed the decondensation procedure described by us recently (25) to avoid problems associated with antigen accessibility in the condensed nuclei. Briefly, total testicular cells obtained from 60-day-old rat were swollen by resuspending them in decondensation buffer containing 0.05 mg/ml heparin (Sigma) and 10 mM dithiothreitol (Sigma) in phosphate buffered-saline (PBS) and incubated in ice for 40 min. Cells obtained after two washes in 1× PBS were processed for indirect immunofluorescence analysis. Mock decondensed cells (incubated in PBS without dithiothreitol and heparin) served as control. Cells were fixed with 4% paraformaldehyde (Sigma) for 20 min followed by permeabilization with 0.1% Triton X-100 (Sigma). 1% bovine serum albumin in PBS was used for blocking nonspecific sites. Localization experiments were carried out by sequentially incubating the smears with primary antibody against TP2 (rabbit polyclonal), acetylated lysine (mouse monoclonal), PCAF (rabbit polyclonal), p300 (rabbit polyclonal), NPM1 (mouse monoclonal), and NPM3 (goat polyclonal); counterstained with corresponding secondary antibodies conjugated with Alexa Fluor 488 and Alexa Fluor 568 Nuclei were stained with DAPI (Sigma). Images were acquired by using a Zeiss confocal laser scanning microscope (LSM 510 META; Carl Zeiss).

MALDI-TOF Analysis of TP2—Endogenous TP2 purified from rat testis was dissolved in 10 μl of deionized water and desalted using a Millipore C4 ZipTip (Millipore, Billerica, MA) with 5 μl of an elution solvent of 50:50 acetonitrile:0.1% trifluoroacetic acid. A 0.3-μl aliquot was placed on the MALDI target, and a 0.5-μl aliquot of a 0.02 μg/μl solution of Promega sequence-grade trypsin in 50 mM ammonium bicarbonate was added. The sample was subjected to on-target tryptic digestion for 1 min, after which 0.5 μl of α-cyano-4-hydroxycinnamic acid matrix (saturated solution in 50:50 acetonitrile:water) was added to the spot, which stopped the enzymatic reaction. Peptide mass spectra were acquired on a Bruker Ultraflex I MALDI-TOF/TOF at the UNC-Duke Proteomics Center (University of North Carolina-Chapel Hill). Data were acquired in the reflectron mode over a scan range of m/z 800–4000. A peptide mass fingerprinting data-base search was performed using the Mascot data-base search engine, allowing six missed cleavages (because of the short digestion time) and with acetylation as a variable modification. Peptide masses were found that matched the following acetylated peptides, but the ions were of too low abundance to be confirmed by tandem mass spectroscopy. To identify the number of residues modified by p300, *in vitro* mass acetylated protein was separated on a 12% SDS-PAGE, the band was excised out, and in-gel protease digestion was carried out in ammonium bicarbonate buffer as described elsewhere (26). V8 protease (Sigma) or trypsin (Sigma) was used for digestion; the resultant peptides were extracted in 50% acetonitrile and 0.1% trifluoroacetic acid, and the peptide masses were analyzed by MALDI-TOF (Bruker Daltonics).

Circular Dichroism (CD) Spectroscopy of Protein-DNA Complexes—Synthetic poly(dG-dC)·poly(dG-dC) (Sigma) was dissolved in Tris-EDTA and dialyzed against CD buffer overnight before use. Circular dichroism spectra of poly(dG-dC)·poly(dG-dC) and its complex with TP2 protein were recorded at room temperature in a buffer containing 10 mM Tris-Cl, pH 7.5, 20 mM NaCl, and 10 μM $ZnSO_4$. The complexes were formed by the addition of buffer, DNA, and finally the protein. The complexes, with increasing protein concentrations, were incubated for 10 min (an increase in the incubation time beyond 10 min did not change the spectra) for each addition of the protein, and the spectra were recorded in a JASCO-810 spectropolarimeter from 300 to 250 nm. The final concentration of the nucleic acids was calculated using the molar extinction coefficients (per mol of phosphate at 260 nm and at 25 °C) and expressed as molar concentration of bases for poly(dG-dC)·poly(dG-dC) = 6350. A mean residue weight of 330 was used for calculating the molar ellipticity of nucleic acids. The change in molar ellipticity observed at 270 nm was plotted as a function of the protein: DNA ratio (mol of protein/base pair). All the nucleoprotein complexes were monitored routinely for absorbance at 400 nm for any light scattering due to aggregation of the complexes; the absorbance was in the range of 0.002 to 0.004.

Atomic Force Microscopy (AFM) Analysis of Nucleoprotein Complexes—Atomic force microscopy was used to visualize TP2-DNA complexes using a 7.2-kb plasmid, p208-12, containing 12 repeats of sea urchin 5s rDNA (27) (a gift from Dr. J. C. Hansen) linearized by digestion with HindIII. All of the samples were dialyzed against buffer containing 10 mM Tris-HCl, pH 8, 1 mM EDTA, and 2.5 mM $MgCl_2$. DNA was spotted on mica and immediately acetylated or mock-acetylated TP2 was added and incubated for 2 min. After washing with deionized water, mica was dried using N_2 gas and processed for imaging using a Nanoscope IV (Digital Instruments) and an RTSP cantilever in air under the tapping mode. The scanning frequency was 1 Hz, and images were captured with the height mode in a 512 × 512-pixel format. The images were processed (plane-fitted and flattened) by the program accompanying the imaging module.

Protein Interaction Studies—To elucidate whether NPM3 and/or NPM1 interacts with TP2, an *in vitro* interaction study was performed as described previously (14) with minor modifications. Briefly, protein-A agarose coupled with anti-TP2 antibodies or preimmune serum were incubated with bacterially expressed TP2 and GST-tagged rat NPM3 or His_6-tagged

human NPM1 in buffer C (20 mM Hepes, pH 7.9, 20% glycerol, 0.2 mM EDTA, 0.2% Triton X-100, and protease inhibitor mixture) for 3–4 h. After washing with buffer C three times, proteins were eluted with SDS sample loading buffer. Proteins were separated in 12% SDS-PAGE, transferred to nitrocellulose membrane, and probed with anti-GST antibody to detect GST-NPM3 and anti-His tag antibody to detect His-NPM1.

To study whether TP2 interacts with NPM3, an *in vivo* immunoprecipitation experiment was performed as follows. Ten microliters of protein A-agarose (Invitrogen) was incubated with 20 μg of either irrelevant antibody or NPM3 monoclonal antibodies in phosphate-buffered saline (137 mM NaCl, 2.7 mM KCl, 10 mM Na_2HPO_4, 2 mM KH_2PO_4, pH 7.4) for 1 h followed by washing once with PBS. Total testicular cell nuclei from a 70-day-old rat was prepared by mincing the testis in PBS followed by homogenization with buffer A (10 mM Hepes, pH 7.9, 1.5 mM $MgCl_2$, 10 mM KCl, 1 mM dithiothreitol, and protease inhibitor mixture (Sigma)). After separating the cytoplasmic and nuclear fractions, the nuclear fractions were lysed in buffer B (20 mM Hepes, pH 7.9, 25% v/v glycerol, 420 mM KCl, 1.5 mM $MgCl_2$, 0.2 mM EDTA, 0.1 mM dithiothreitol, and protease inhibitor mixture). Salt concentration was adjusted to 150 mM by diluting the mixture in buffer C. Nuclear lysate was precleared with protein A-agarose beads followed by incubation with antibody coupled beads for 3–4 h and then by three washes with buffer C. The bound proteins were separated on SDS-12% PAGE, transferred onto nitrocellulose membrane, and probed with anti-TP2 antibody to detect immunoprecipitated TP2.

To identify the TP2 domain interacting with NPM3, a peptide pulldown assay was performed as follows. five μg each of the chemically synthesized biotin-conjugated TP2 peptides were allowed to bind to immobilized avidin beads (Pierce) in PBS for 1 h. Beads bound to biotinylated peptides were incubated with 2 μg of GST-NPM3 in buffer C for 3–4 h at 4 °C, followed by three washes with the same buffer. The bound proteins were separated on SDS-12% PAGE, transferred onto nitrocellulose membrane, and probed with anti-GST antibody to detect precipitated GST-NPM3.

GST pulldown assays were performed to study the effect of acetylation on TP2 with NPM3 interaction. GST-NPM3 and GST proteins were immobilized to glutathione-agarose beads (Sigma) in phosphate-buffered saline (containing 137 mM NaCl, 2.7 mM KCl, 10 mM Na_2HPO_4, 2 mM KH_2PO_4, pH 7.4) for 1 h at 4 °C. Glutathione-agarose 4B beads coupled with GST and GST-NPM3 were incubated with acetylated or mock-acetylated recombinant TP2 in buffer C and incubated at 4 °C for 4 h followed by three washes with the same buffer. Bound fractions were separated on SDS-12% PAGE, and TP2 was detected by Western blot analysis with anti-TP2 monospecific antibody.

Real-time PCR Analysis—Real-time PCR analysis was performed as described previously (14). The primers used were as follows: NPM1 (GenBank™ accession number NM_012992) forward primer, 5′-ccacctgtggtcttgaggtt-3′, and reverse primer, 5′-tcttgacccttgaccttgg-3′; NPM3 (GenBank™ accession number XM_001058548) forward primer, 5′-gaacatgtgctggcttgaa-3′, and reverse primer, 5′-gcaggaaggattccacacag-3′. Differences in Ct (threshold values) were used to calculate -fold difference in expression of mRNA in gametic diploid (2n) Tetraploid (4n) and haploid (n) cells by the Delta-Delta Ct method ($2^{\text{delta-delta Ct}}$) of analysis. NACA (nascent polypeptide-associated complex α) was used as an internal normalization control, as its expression level across different stages of germ cell differentiation was found to be unaltered in our microarray experiments.

RESULTS

As mentioned earlier, acetylation/deacetylation of histones plays a major role in many of the chromatin-mediated functions including the histone replacement process in mammalian spermiogenesis (18, 19). Although genetic studies have clearly shown that the two transition proteins TP1 and TP2 are essential for the generation of viable spermatozoa, the molecular mechanism involved in the deposition of these transition proteins on spermatid chromatin, histone displacement, and their subsequent replacement by protamines are rather poorly understood. We were curious to examine whether transition protein 2 also gets acetylated during spermiogenesis.

For this purpose, we carried out analysis with acetylated lysine antibody to detect the presence of acetylated TP2 in rat spermatids. 5–25% trichloroacetic acid precipitate fractions of the acid extract of the sonication-resistant nuclei (representing elongating and elongated spermatids) were probed with anti-acetylated lysine antibody (Fig. 1*A*). Anti-acetylated lysine antibody picked up only *in vivo* TP2 (Fig. 1*A*, *lane 3*) band but not TP1 (*bottom band* in *lane 3*) and bacterially expressed TP2 (*lane 2*), indicating the presence of *in vivo* acetylated TP2. An intense signal in the 5% trichloroacetic acid precipitate of sonication-resistant spermatid acid extract (Fig. 1*A*, *lane 1*) shows the presence of hyperacetylated H4 in the elongating spermatids as reported earlier (19).

We also carried out indirect immunofluorescence experiments to see whether anti-acetylated lysine antibody colocalizes with TP2 in different stages of maturation of spermatids. For this purpose, we used the decondensation method described by us recently (25) to make sure that antigen accessibility for the antibody was not masked because of the condensed nature of the nuclei. The confocal analysis shown in Fig. 1*B* reveals the presence of partial colocalization between acetylated lysine and TP2. Interestingly, we observed that acetylated lysine signal was not present in late condensing spermatids, suggesting that acetylation of TP2 is stage-dependent (Fig. 1*B*, *panel 5*). The scatter plot analysis of Fig. 1*B*, *panel 3*, is shown in Fig. 1*C*, wherein we have also shown the cut mask image (*panel II*). Fig. 1*C*, *panel III*, represents the number of pixels in the three scatter regions.

To identify the *in vivo* acetylation sites on transition protein 2, we purified TP2 from the rat testis as described under "Materials and Methods." On-target trypsin digestion of TP2 followed by MALDI-TOF analysis gave several peaks out of which one peptide corresponds to the acetylated peptide of TP2. The acetylated peptide, along with the mass changes, is given in Fig. 1*D*. We detected the peptide GSCPKNRKTLEGKVSKRK with one acetylated lysine residue. Because TP2 has several lysine and arginine residues, it was very difficult to characterize all of

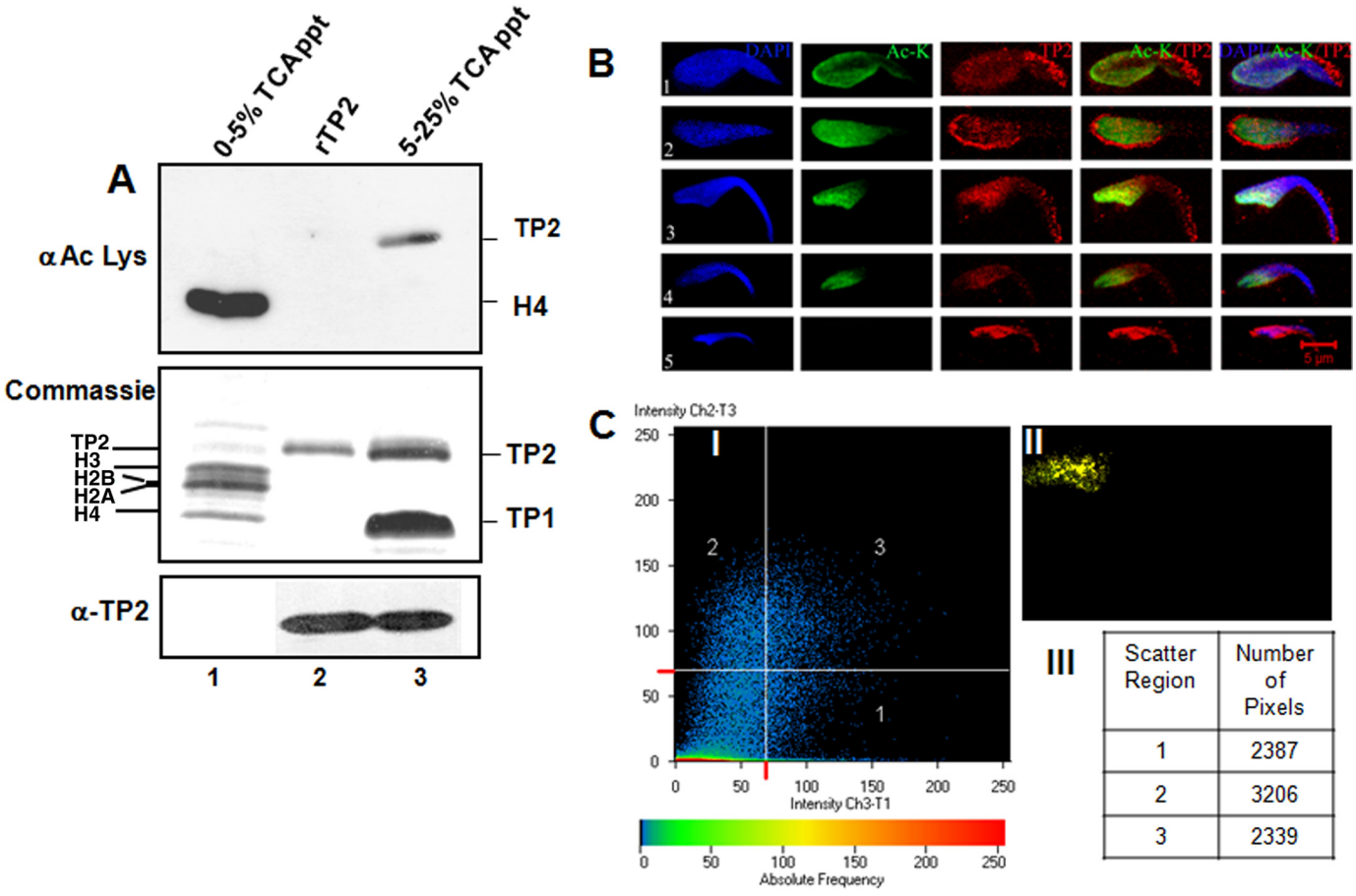

FIGURE 1. **TP2 is acetylated *in vivo*.** *A*, Western blot analysis with acetyllysine antibody. Proteins from 0–5% and 5–25% trichloroacetic acid precipitate of acid-soluble fractions of sonication-resistant nuclei of rat testis were run in duplicate on 12% SDS-PAGE, transferred to a polyvinylidene difluoride membrane, and probed with anti-acetylated lysine antibody (*top panel*) or anti-TP2 antibody (*bottom panel*). The *middle panel* represents a Ponceau pattern of proteins. *Lane 1* is core histones enriched in 5% trichloroacetic acid precipitate (*TCA*). *Lane 2* is recombinant TP2, and *lane 3* is endogenous rat TP2. *B*, localization of endogenous TP2 and acetylated lysine residue in decondensed spermatids. Decondensation of spermatids was carried out as described under "Materials and Methods." Indirect immunofluorescence was carried out with mouse anti-acetylated lysine antibody and rabbit anti-TP2 antibody. *Panels 1–5* represent spermatids at different stages of maturation. *Columns* from *left* to *right* show the fluorescence patterns of DAPI, Ac-K, TP2, Ac-K/TP2 overlay, and a merged (DAPI/Ac-K/TP2) image. *C*, analysis of the colocalized area of TP2 and Ac-K using Zeiss software. *Panel I* represents scatter plot generated for *B*(*3*) showing TP2 (scatter region *1*), Ac-K (scatter region *2*), and colocalized pixels (scatter region *3*) in the image. *Panel II* represents the cut mask area showing only colocalized pixels in the image. The *table* (*panel III*) depicts the number of pixels in the three scatter regions. *D*, acetylation status of *in vivo* TP2. MALDI-TOF analysis of *in vivo* TP2 upon on-target digestion with trypsin for 1 min yielded many peaks, of which one peptide (amino acids 76–93) corresponds to the peptide mass in addition to the mass for a single acetyl group.

the lysine modifications of the trypsin-derived peptides. Furthermore, we were not able to sequence the peptides or TP2 protein itself because of several technical problems associated with the ionization. Despite these difficulties, the peptide with acetylated lysine residue indicates that the acetylation domain is in the C terminus of the protein.

p300/CBP and PCAF Acetylate TP2 in Vitro—After establishing that acetylation of TP2 does occur *in vivo*, we went ahead to identify the enzyme involved in the acetylation of TP2. Among the several known lysine acetyltransferases, p300/CBP and PCAF acetylate many non-histone proteins in addition to nucleosomal core histones. Therefore, we checked whether these two enzymes could acetylate TP2 *in vitro*. For this purpose full-length His_6-tagged p300 and FLAG epitope-tagged PCAF from respective baculovirus-infected Sf21 cells were purified and used as the enzyme source. The highly purified human core histones isolated from the HeLa nuclear pellet were used as a positive control, and NAP1 was used as a negative control. As seen on Fig. 2*A*, both p300 and PCAF could acetylate recombinant TP2 as monitored by the filter binding assay. Comparatively, the efficiency of acetylation of TP2 was much higher with p300 than with PCAF. Acetylation was also confirmed by SDS-PAGE and subsequent autoradiography as shown in Fig. 2*B*. We also observed that the paralog of p300, namely CBP, also acetylates TP2 with equal efficiency (data not shown).

Initially we carried out real-time PCR analysis of p300 and PCAF in diploid, tetraploid and haploid spermatogenic cells. The tetraploid (4n) and haploid (n) germ cells were purified

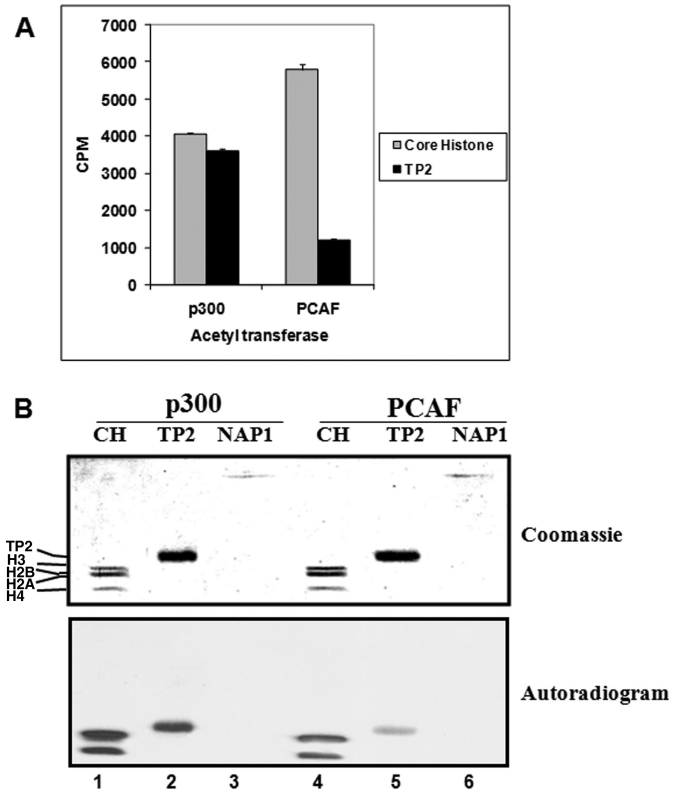

FIGURE 2. **TP2 gets acetylated *in vitro* by p300 and PCAF.** *A*, after acetylation of 800 ng of TP2 and core histones by p300 and PCAF in an *in vitro* reaction using 0.5 μl of [^{3}H]acetyl coenzyme A (3.3 Ci/mmol), the entire reaction mixture was spotted on P-81 filter paper, and radioactive counts were taken. The *gray bar* indicates cpm for core histones, and the *black bar* indicates cpm for TP2. *B*, after an *in vitro* acetylation reaction with p300 (*lanes 1–3*) and PCAF (*lanes 4–6*), protein samples were precipitated by 25% trichloroacetic acid, washed with chilled acetone, loaded on 15% SDS-PAGE, and stained with Coomassie Blue (*upper panel*) or exposed to x-ray film for autoradiography (*lower panel*). Acetylation reaction was performed for core histones (*CH*, *lanes 1* and *4*) and TP2 protein (*lanes 2* and *5*); NAP1 served as a negative control (*lanes 3* and *6*).

from rat testis by the technique of centrifugal elutriation, and testicular cells from 10-day-old rats served as the source of diploid germ cells. The isolated tetraploid and haploid germ cells as checked by fluorescence-activated cell sorter (FACS) analysis (14) were ~80 and 95% pure, respectively. Fig. 3*A* shows the relative abundance of p300 and PCAF transcripts in gametic diploid (spermatogonia), tetraploid (spermatocytes), and haploid spermatids cells. Subsequently, we carried out indirect immunofluorescence analysis of decondensed spermatids with p300 and PCAF antibodies, as shown in Fig. 3, *B* and *C*, respectively. As seen, both of these proteins are present at all stages of condensing spermatids. We also carried out Western blot analysis of total testicular nuclear extract and nuclear extract of sonication-resistant nuclei to show the presence of PCAF in these nuclei (Fig. 3*D*). In the sonication-resistant spermatid nuclear extract we observed a single band corresponding to PCAF (Fig. 3*D*, *lane 2*), whereas in the total testicular nuclear extract we also detected higher molecular mass bands in addition to the expected 89-kDa band (*lane 1*). These additional higher molecular mass bands probably reflect aggregated forms of PCAF. For the detection of p300 in the nuclei of elongating and elongated spermatids (sonication-resistant spermatids), we resorted to Western analysis of the immunoprecipitated complex because it is reported in the literature to be very difficult to detect p300 directly in a Western blot analysis. Fig. 3*E* shows that we detected p300 in the immunoprecipitated complex obtained from p300 antibodies but not in preimmune serum. p300 also exists as a multiprotein complex *in vivo* associating with several ancillary factors. Thus, to establish that the *in vivo* p300 protein complex can acetylate TP2, the immunoprecipitated p300 complex was used as the enzyme source for carrying out acetylation reactions with TP2 as the acceptor protein. As can be seen in Fig. 3*F*, the p300-enriched immunocomplex acetylated TP2 *in vitro*. Fig. 3*F* also shows that the immunocomplex can acetylate the nucleosomal core histones as expected.

TP2 Is Acetylated in the C-terminal DNA-condensing Domain—To map the TP2 domain that is acetylated *in vitro* by p300, *in vitro* acetylated TP2, using [^{3}H]acetyl coenzyme A (3.3 Ci/mmol), was digested with V8 protease, which cleaves TP2 into two fragments, the N-terminal zinc finger domain and the C-terminal DNA condensing domain (8, 28). The protease digest was run on a 15% acid urea PAGE and stained with Amido Black to visualize the N-terminal domain (migrates toward the top) and C-terminal domain (migrates toward the bottom) (Fig. 4*A*). The autoradiography of the gel showing the C-terminal domain of TP2 is predominantly acetylated compared with N-terminal domain (Fig. 4*B*, *lane 1*). In Fig. 4*B*, *lane 2* shows an acetylation signal for undigested TP2. We carried out bulk acetylation of TP2 using cold acetyl coenzyme A and p300, and the V8 protease-derived C-terminal fragment was then subjected to MALDI-TOF analysis to identify the number of lysine residues that were modified in the C-terminal domain. MALDI-TOF showed five peaks with a difference of 42 daltons (Fig. 4*C*) in which peak 1 is an unacetylated, peak 2 a monoacetylated, peak 3 a diacetylated, peak 4 a triacetylated, and peak 5 a tetraacetylated peptide. Then we also used a synthetic peptide corresponding to C-terminal domain and analyzed the p300-mediated acetylated products by MALDI-TOF analysis (Fig. 4*D*). Peaks similar to those shown in Fig. 4*C* were detected. It is interesting to note that the acetylated peptide partially covering the C-terminal domain was also detected by MALDI-TOF analysis of the *in vivo* TP2 (Fig. 1*D*).

A multiple protein sequence alignment of TP2 from 10 known mammalian species shows a high degree of conservation of four lysines in the C-terminal domain of TP2 beyond the V8 protease cleavage site (shown in Fig. 4*E*); this could be the target of acetylation by p300.

Effect of Acetylation on TP2-mediated DNA Condensation—TP2 is a DNA-condensing protein showing a sequence preference for alternating GC-rich sequences (10, 28). We had earlier delineated the two structural and functional domains of TP2, the N-terminal one-third having two zinc finger modules and the C-terminal one-third, which is basic in nature, having a DNA condensation property (8). The results presented above clearly show that TP2 is acetylated by p300 in its C-terminal basic domain. Hence, our next aim was to determine the effect of acetylation on the DNA condensing property of TP2. For this purpose, acetylated TP2 was obtained by incubating recombinant TP2 with p300 in the presence of cold acetyl-CoA. This acetylation of TP2 by p300 is nearly complete, as shown by the

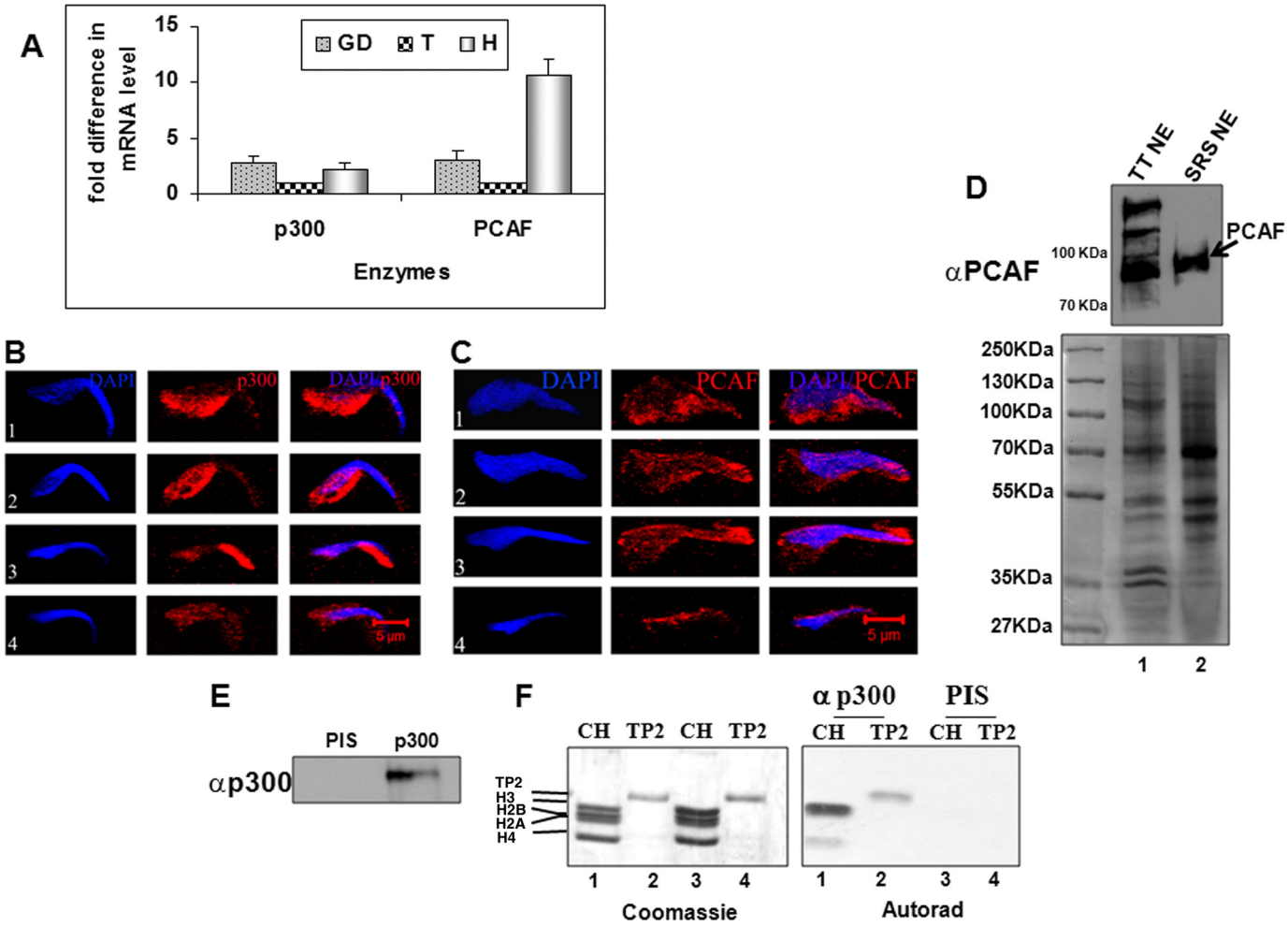

FIGURE 3. **Presence of p300 and PCAF in condensing spermatids and acetylation of TP2 by immunoprecipitated p300 complex from haploid spermatid nuclear extract.** *A*, real-time PCR analysis of p300 and PCAF in spermatogenic cells. Tetraploid and haploid germ cells were isolated from rat testis using a centrifugal elutriation technique. Testicular cells from 10-day-old rats represented gametic diploid cells. -Fold differences in the expression of p300 and PCAF were compared in tetraploid, haploid, and gametic diploid cells keeping the low expressing cells as the reference. NACA1 was used as a normalization control. *GD*, gametic diploid; *T*, tetraploid; *H*, haploid germ cells. *B* and *C*, indirect immunofluorescence analysis of condensing spermatids was carried out with polyclonal anti-p300 and rabbit polyclonal anti-PCAF antibodies, respectively. *Panels 1–4* represent decondensed condensing spermatids at different stages of maturation. *Columns* from *left* to *right* show fluorescence patterns of DAPI, p300/PCAF, respectively, and a merged image. *D*, Western blot analysis showing the presence of PCAF protein. Proteins from total testicular nuclei and sonication-resistant nuclei of 60-day-old rat testis were run in duplicate on an 8% gel (Coomassie-stained gel (*lower panel*)), then transferred to a nitrocellulose membrane and probed with anti-PCAF antibody (*upper panel*). *Lanes 1* and *2* are nuclear extract from total testicular cells and sonication-resistant cells, respectively. *E*, p300 complex from the haploid spermatids were immunoprecipitated with monoclonal anti-p300 antibodies, and the immunoprecipitated proteins were probed with polyclonal anti-p300 antibody. Preimmune serum (*PIS*) served as control. *F*, immunoprecipitated p300 complex on beads were used as the enzyme source for acetylation reaction using core histone (*CH*) (*lane 1*) and recombinant TP2 (*lane 2*) as substrates. Immunoprecipitates obtained with preimmune sera (*lanes 3* and *4*) were used as control for the acetylation reaction. The *left panel* shows core histone and TP2 substrates run in duplicates and stained with Coomassie Blue, and the *right panel* shows the autoradiogram.

retarded mobility of acetylated TP2 in an acid urea PAGE (Fig. 5*A*). To determine the effect of acetylation on the DNA condensation properties of both acetylated TP2 and mock acetylated TP2, we used circular dichroism spectra, which we had used earlier to characterize the DNA condensation property of TP2. Because TP2 condenses DNA in a GC-rich sequence specific-manner, we used double-stranded poly(dG-dC)·poly(dG-dC) DNA in these studies (10). The series of spectra shown in Fig. 5*B* shows that adding increasing concentrations of TP2 resulted in a progressive decrease in positive ellipticity at 270 nm, which is in conformity with our earlier observations. However, when we used acetylated TP2 at the same concentration, The DNA condensation as monitored by θ at 270 nm was much less as compared with mock acetylated TP2 (Fig. 5*C*). The difference in the compaction of DNA ($\Delta\theta$ values) at 270 nm was plotted as a function of an increasing protein to DNA ratio in terms of mol of protein/base pair (shown in Fig. 5*D*). Thus, the *in vitro* DNA condensation studies using a CD spectroscopy technique demonstrated that acetylation of TP2 reduces TP2-mediated DNA condensation.

Atomic Force Microscopy (AFM) Visualization of TP2 and Acetylated TP2-DNA Complexes—Circular dichroism spectroscopy measures only the optical property of nucleic acids. However, the more recently developed technique of AFM provides the opportunity to visualize directly the higher ordered packaging of DNA by histones (29, 30). Hence we used this technique to observe the effect of the acetylation of TP2 on its DNA condensation property. For this purpose we complexed DNA with either mock acetylated TP2 or acetylated TP2. The AFM images were captured as described under "Materials and

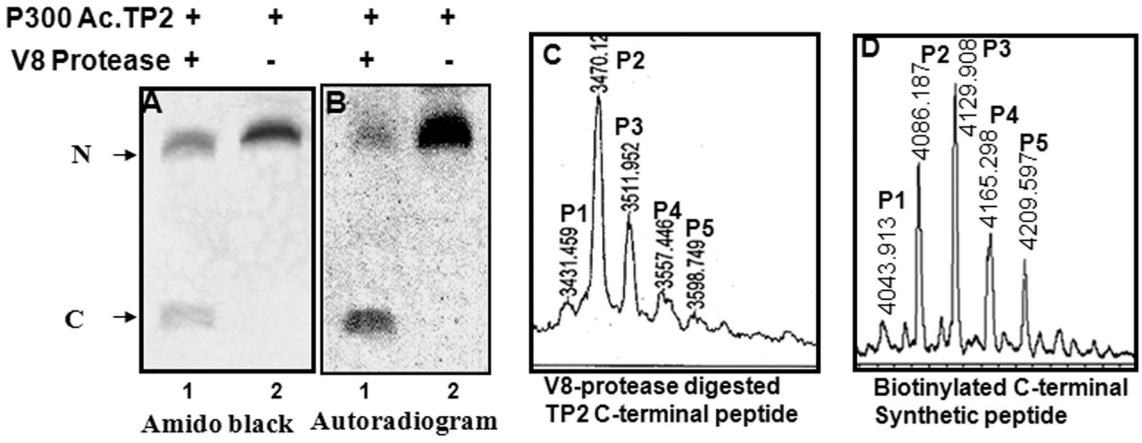

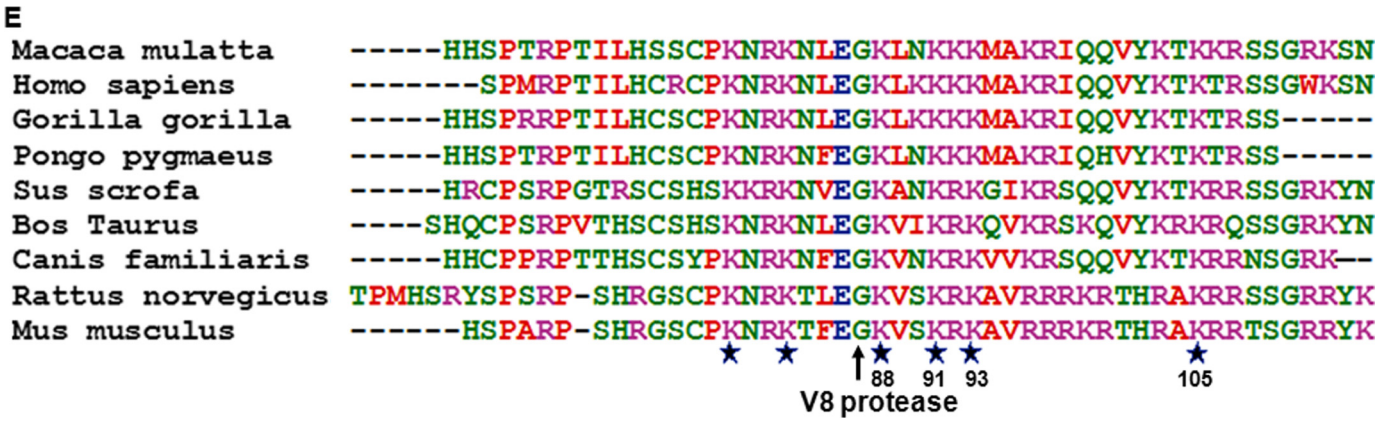

FIGURE 4. **TP2 is acetylated predominantly in the C-terminal basic domain.** *A* and *B*, after *in vitro* acetylation with p300 and [^{3}H]acetyl-CoA, TP2 protein was precipitated with 25% trichloroacetic acid and digested with V8 protease in ammonium bicarbonate buffer as described under "Materials and Methods." The Protein digest was electrophoresed on 15% acid urea PAGE, stained with Amido Black, and exposed for autoradiography. *A*, Amido Black-stained gel. *B*, autoradiography of the same gel. *Lane 1* in both *A* and *B* shows V8 protease-derived N- and C-terminal fragments of TP2, and *lane 2* represents undigested acetylated TP2. *C*, after *in vitro* acetylation of TP2 with p300 and cold acetyl-CoA, TP2 protein was precipitated with trichloroacetic acid and digested with V8 protease in ammonium bicarbonate buffer, and the C-terminal fragment was analyzed by MALDI-TOF. *D*, biotinylated synthetic TP2 C-terminal peptide was acetylated with p300 and cold acetyl coenzyme A, precipitated by 25% trichloroacetic acid, and subjected directly to MALDI-TOF. Unacetylated (peak 1 (*p1*)), monoacetylated (peak 2 (*p2*)), diacetylated (peak 3 (*p3*)), triacetylated (peak 4 (*p4*)), and tetraacetylated (peak 5 (*p5*)) peptides are shown. *E*, the amino acid sequences of TP2 in its C-terminal domain from different mammalian species and four conserved lysine residues, which are potential sites of acetylation are shown.

Methods" and are shown in Fig. 5, *E–G*. Incubation of the mock acetylated TP2 formed compact globular condensate structures (Fig. 5*F*). On the other hand, in agreement with the CD spectroscopic data, the addition of acetylated TP2 to the DNA had no visual effect on the folding of the DNA molecules (Fig. 5*G*). Fig. 5*H* shows a high resolution image of DNA condensate (*arrowhead*) and condensation intermediate (*arrow*) observed upon the incubation of mock acetylated TP2 with DNA.

Nucleoplasmin 3 (NPM3) Interacts with TP2 in Vitro and in Vivo—The transition proteins, histone H1 variants (H1LS and H1T2), and protamines that are expressed and deposited onto chromatin in a DNA replication-independent manner during spermiogenesis are very basic in nature. These proteins could be deleterious to cells through self-aggregation and promiscuous interactions with nucleic acids and other proteins. It is becoming increasingly clear that when histones are not in association with DNA they bind to dedicated proteins called histone chaperones. We do not have any information at present as to the natural chaperones involved in the replacement of histones by transition proteins or the final replacement of transition proteins by protamines. Identification of chaperones associated with TPs should give valuable insights into the storage, assembly, and replacement of these basic nuclear proteins during spermiogenesis. Although HSPA2 was identified as the first transition protein chaperone in postmeiotic haploid spermatids, the function of this chaperone needs to be addressed (31). We looked at NPM1 and NPM3 as possible candidates for the nuclear chaperone involved in global replacement process during spermiogenesis. It has been reported that NPM3 is highly expressed in the testis compared with other tissues (32). NPM3 was also detected in a proteomic analysis of acid-soluble proteins present in sonication-resistant spermatid nucleus (31). Therefore, we initially carried out the expression level analysis of NPM3 in haploid spermatids, as the original report of MacArthur and Shackleford (32) studied the expression of NPM3 in total testis.

Our results from real-time PCR analysis showed that NPM3 is up-regulated ~6 fold in meiotic and postmeiotic haploid cells compared with gametic diploid cells. On the other hand, the nucleoplasmin 1 (NPM1/B23) (nucleoplasmin or nucleophosmin) mRNA expression level was not significantly altered in these germ cells (Fig. 6*A*). Further, the presence of NPM1 and

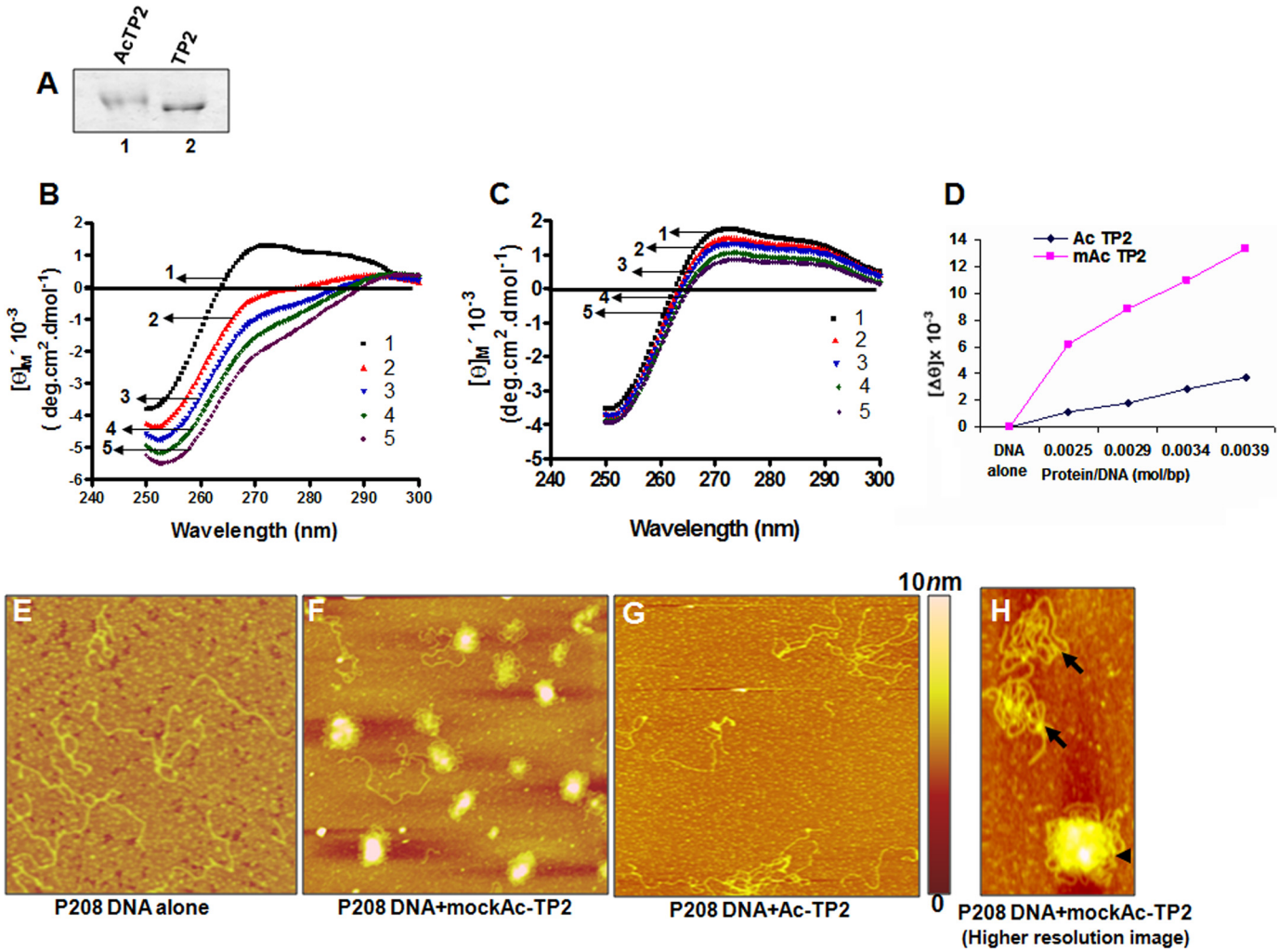

FIGURE 5. **Effect of acetylation on the DNA condensation properties of TP2.** *A*, 15% acid urea PAGE showing the difference in mobility between TP2 and acetylated TP2 (*AcTP2*) (3 μg each) stained with Amido Black. *B* and *C*, circular dichroism spectroscopy of poly(dG-dC)·poly(dG-dC) with increasing concentrations of mock acetylated TP2 (*B*) and acetylated TP2 (*C*), respectively. *1*, DNA alone; *2*, DNA + TP2 (protein to nucleotide ratio 0.0025); *3*, DNA + TP2 (protein to nucleotide ratio 0.0029); *4*, DNA + TP2 (protein to nucleotide ratio 0.0034); *5*, DNA + TP2 (protein to nucleotide ratio 0.0039). *D*, comparison of Dθ values of mock acetylated TP2-DNA and acetylated TP2-DNA complexes at 270 nm. *E*, AFM image of linearized plasmid p208-12 rDNA molecules showing the DNA fiber on mica without the addition of TP2. *F* and *G*, TP2-DNA complexes formed by first loosely attaching the DNA to the mica surface and then adding mock acetylated (*E*) and acetylated TP2 (*F*), respectively, to form complexes. *H*, high resolution image of TP2-DNA complexes showing different stages of TP2-DNA complex formation.

NPM3 in sonication-resistant nuclei was confirmed by Western blot analysis (Fig. 6*B*). Subsequently we carried out physical interaction studies to examine the interaction of NPM1 and NPM3 with TP2 using recombinant proteins GST-NPM3 and TP2. The GST-NPM3 pulldown experiment clearly showed that TP2 does interact physically with NPM3 *in vitro* (Fig. 6*C*, *lower panel*). We also carried out physical interaction studies with human NPM1 (90% identity with rat NPM1), and the results shown in Fig. 6*C* (*upper panel*) clearly reveal that NPM1 does not interact with TP2. To further provide evidence that NPM3 interacts with TP2 *in vivo*, we carried out an immunoprecipitation experiment with anti-NPM3 antibodies with nuclear extract from sonication-resistant nuclei. After separating the immunoprecipitated products on an SDS-12% PAGE and transferring them onto membrane, we probed the blot with TP2 antibody. The results presented in Fig. 6*D* clearly show that TP2 was detected in the immunoprecipitated complex. Such interaction was not detected in a control experiment using preimmune serum instead of NPM3 antibodies in the immunoprecipitation experiment. We then carried out indirect immunofluorescence experiments to examine the colocalization of TP2 and NPM3 in condensing spermatids. The indirect immunofluorescence results reveal that the majority of the pixels of NPM3 colocalized with TP2 in elongating spermatids (Fig. 6*E*).

To identify the TP2 domain that interacts with NPM3, a GST-NPM3 pulldown experiment was done with synthetic peptides covering the N-terminal, middle, and C-terminal regions as described under "Materials and Methods." The results show that NPM3 interacts with the C-terminal peptide of TP2 (Fig. 7*C*, *lane 4*) with high affinity compared with the N-terminal peptide (*lane 2*) and middle peptides (*lane 3*).

As we have demonstrated in the present study that TP2 is acetylated in its C-terminal domain, we next raised the question of the effect of acetylation on its interaction with the histone chaperone NPM3. An interaction study was performed with increasing amounts of TP2, as shown in Fig. 7*D*, and 2 μg of

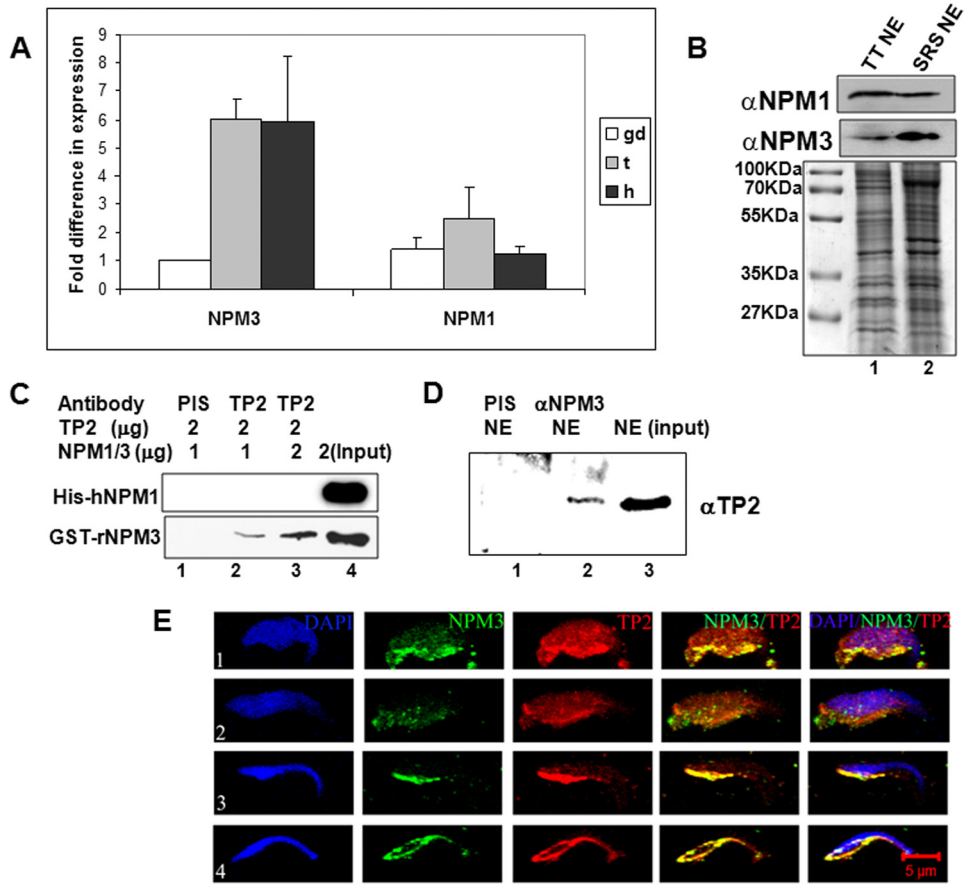

FIGURE 6. **Up-regulated NPM3 interacts with TP2 *in vitro* and *in vivo*.** *A*, real-time PCR analysis of histone chaperones NPM3 and NPM1. NACA1 was used as a normalization control. -Fold differences in expression of NPMs were compared in tetraploid haploid and gametic diploid cells keeping low expressing cells as the reference. *gd*, gametic diploid; *t*, tetraploid; *h*, haploid germ cells. *B*, Western blot analysis showing the presence of NPM1 and NPM3. Proteins from total testicular nuclei and sonication-resistant nuclei of 60-day-old rat testis were run in duplicate on a 12% gel (Coomassie-stained gel (*lower panel*)), then transferred to a nitrocellulose membrane and probed with anti-NPM1 antibody and anti-NPM3 antibody (*upper panel*). *Lanes 1* and *2* are nuclear extract from total testicular cells and sonication-resistant cells, respectively. *C*, physical interaction of TP2 with NPM1 and NPM3. Recombinant TP2 (3 μg), incubated separately with 3 μg of GST-tagged rat NPM3 and His-tagged human NPM1, was then bound to protein A-agarose beads coupled with anti-TP2 antibodies raised in goat. Preimmune sera (*PIS*) bound to protein A-agarose beads (*lane 1*) and TP2 antibody without TP2 protein (*lane 2*) were used as negative control. The interacting proteins were analyzed by Western blot analysis using anti-GST antibodies for GST-NPM3 and anti-His tag antibodies (His-NPM1). *D*, immunoprecipitation of TP2 from testicular nuclear extract (*NE*) using NPM3 antibody (*lane 2*). The immunoprecipitated complex was separated in 12% SDS-PAGE, and the proteins were transferred on to nitrocellulose membrane and probed with anti-TP2 antibody. *Lane 3* shows the input nuclear extract, and *lane 1* shows the experiment carried out using preimmune serum as the control. *E*, localization of endogenous TP2 and NPM3 in decondensed condensing spermatids. *Panels 1–4* represents decondensed spermatids at different stages of maturation. *Columns* from *left* to *right* show fluorescence patterns of DAPI, NPM3, TP2, NPM3/TP2 overlay, and the merged (DAPI/NPM3/TP2) image.

GST/GST-NPM3. The results show that acetylation on TP2 significantly decreases its affinity to NPM3 (Fig. 7*D*).

DISCUSSION

Histone acetylation/deacetylation catalyzed by histone acetyltransferases and histone deacetylases is an important mechanism for the regulation of gene expression in eukaryotic cells. More recently, it is becoming clear that acetylation also occurs on several non-histone proteins; this modification is associated with several phenomena other than the transcription process (reviewed in Ref. 17). Mammalian spermiogenesis is a process in which haploid round spermatids mature and are transformed into highly condensed and transcriptionally inert spermatozoa involving 1–19 stages. This system is a fascinating model of the global chromatin remodeling process in which histones and their variants are replaced initially by transition proteins TP1, TP2, and TP4 during stages 12–15, and these are subsequently replaced by the protamines during stages 15–19. Hyperacetylation of histone H4 has been reported to occur during stages 10–12 and is believed to be associated with or facilitate the removal/replacement of histones by the transition proteins (19). However, there has been no report on posttranslational modifications on transition proteins other than phosphorylation of TP2 (13). The present work was initiated to strengthen our *in vitro* results based on reaction with anti-acetylated lysine antibodies as well as mass spectrometric analysis, which clearly showed that TP2 is acetylated *in vivo*. These *in vivo* data were further corroborated by our *in vitro* experiments using the histone acetyltransferases p300 and PCAF. The acetylation of TP2 by p300 was three times more efficient than PCAF. Because both p300 and PCAF are present in the elongating spermatids, it is difficult for us to conclude, at present, which of these two histone acetyltransferases acetylates TP2 *in vivo*. It is interesting to note that acetylation of TP2 is localized predominantly to the C-terminal basic domain. We detected up to a tetraacetylated C-terminal fragment from the *in vitro* acetylation reaction as revealed by mass analysis in a MALDI-TOF. These acetylation data on C-terminal peptides were also further corroborated by the acetylation of synthetic peptides corresponding to the C-terminal domain catalyzed by p300. Although we have not mapped the exact acetylation sites in the C-terminal fragment experimentally, the conservation of four lysine residues in TP2 from other mammalian species suggests that lysines 88, 91, 93, and 105 are the most probable sites of acetylation. Although we detected tetraacetylated TP2 from an *in vitro* p300-mediated acetylation reaction, we detected only monoacetylated TP2 isolated from testis. It is quite possible that acetylation of TP2 is a dynamic process, which is also context-dependent in the total process of global chromatin remodeling occurring at this stage of spermiogenesis.

We next asked the question, what is the functional significance of acetylation of TP2? An established molecular property

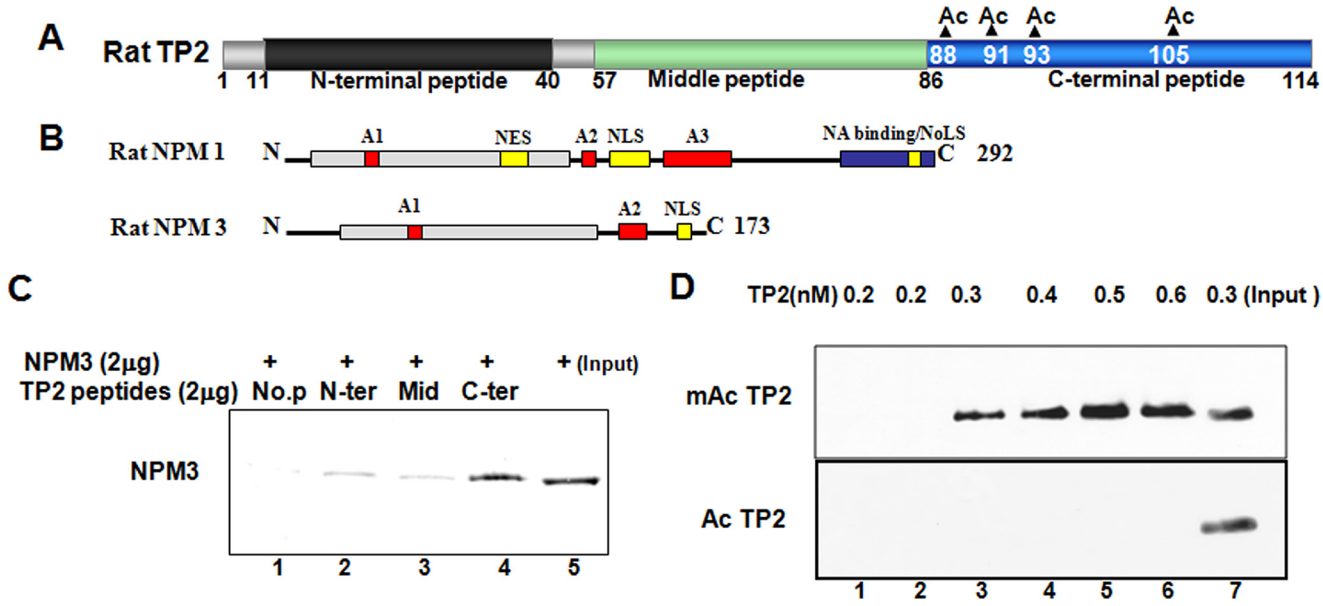

FIGURE 7. **NPM3 interacts with C-terminal domain of TP2.** *A*, diagrammatic representation of regions of TP2 used for synthesizing biotinylated peptide N-terminal peptide (shown in *black*). The middle peptide and the C-terminal peptides are shown in *green* and *blue*, respectively. The four putative acetylation sites in the C terminus are *numbered*. *B*, depiction of the NPM1 and NPM3 protein domains in which acid stretches are shown in *red*. Localization signals are shown in *yellow* (*NLS*, nuclear localization signal; *NES*, nuclear export signal; *NoLS*, nucleolar localization signal). The core domains are shown in *gray*. NPM1 members have a nucleic acid (*NA*) binding domain at the C terminus, which is shown in *blue*. *C*, NPM3 interacts with C-terminal domain of TP2. Biotin-conjugated synthetic peptides of TP2 were bound to streptavidin beads and incubated with GST-NPM3. The captured proteins were probed with anti-GST antibodies. NPM3 was efficiently bound to the C-terminal peptide of TP2 (*lane 4*) compared with the N-terminal (*lane 2*) and middle TP2 peptide (*lane 3*); beads alone were used as control (*lane 1*). *D*, acetylation of TP2 blocks its interaction with NPM3. 0.5 nM GST (*lane 1*) and 0.5 nM GST NPM3 (*lanes 2–6*) was coupled to glutathione-agarose. Increasing concentrations of mock acetylated and acetylated TP2 (*lanes 1* and *2*, 0.2 nM; *lane 3*, 0.3 nM; *lane 4*, 0.4 nM; *lane 5*, 0.5 nM; *lane 6*, 0.6 nM) were incubated with the beads, and the pulled down proteins were separated on 12% SDS-PAGE and probed with TP2 antibody.

of TP2 is its DNA condensation ability, manifested through its basic C-terminal domain (28, 8), which has been substantiated by the mouse knock-out studies of Meistrich and co-workers (6). Thus we embarked upon the study of the effect of acetylation of TP2 on its DNA condensation property. The results presented in Fig. 5, describing the circular dichroism spectroscopic studies as well as visualizing the protein-DNA complex by AFM (Fig. 5) clearly show that acetylation drastically reduces the DNA condensation property of TP2. However, we cannot ascertain at present the relevance of this acetylation-dependent lack of condensation in the total process of chromatin remodeling occurring at these stages. It is possible that local decondensation resulting from acetylation of TP2 might facilitate the DNA repair activity associated with the repair of several strand breaks in the genome that occur during these stages of spermiogenesis (33).

Another important aspect of the present investigation is the identification NPM3 as an interacting protein of TP2. We were stimulated to carry out the experiment based on the observations of MacArthur and Shackleford (32) that showed up-regulation of expression of NPM3 in the total testis as compared with other tissues. In the present article, we went further and showed a higher expression of NPM3 in tetraploid and post-meiotic haploid cells; the NPM3 protein is also detected in elongating spermatids. NPM3 belongs to the nucleophosmin/nucleoplasmin (NPM) family of proteins, which includes NPM1 and NPM2. It is now clearly established that NPM1 (B23) has histone chaperone activity (reviewed in Ref. 34). The N-terminal core is the most conserved domain between these proteins and, in most cases, includes a short A1 acid tract, which is responsible for oligomerization and chaperone activity. A second region, the C-terminal tail domain, contains up to two additional acids tracts (A2 and A3) and has variable lengths and functional motifs between the family members (Fig. 7*B*). For NPM1, the A3 region is the longest of the three acid tracts, and it is completely absent in NPM3. However, the A2 domain is longer in NPM3 compared with NPM1 (34). In contrast to the histone binding domain, the nucleosome assembly function is localized to the C terminus and to the last acid tract. The chaperone activity of mammalian NPM3 is not well characterized. By a genetic screen in yeast, human NPM3 was shown to interact with human NPM1, suggesting that NPM3 may form a hetero-oligomer with NPM1 (35) *Xenopus* NPM3 has also been shown to be immunoprecipitated along with NPM1 (36). However, an independent function of NPM3 without NPM1 cannot be ruled out at present. The existing evidence suggests a role for NPM3 in rDNA transcription in the nucleolus (35). Although a role for NPM3 in the decondensation of sperm chromatin in *Xenopus* has been suggested, the effect of the antisense oligo used in these studies on the levels of other NPMs has not been clearly demonstrated (reviewed in Ref. 34). NPM3 is known to interact with the histone H4 tail, which is rich in basic amino acids (37). Interestingly, we also saw a high affinity of binding to the C-terminal domain of TP2, which is also basic in nature. Therefore, interaction of NPM3 with the C-terminal basic domain of TP2 raises the question of whether this interaction with the acidic stretches of NPM3 is purely electrostatic in nature. However, this is very unlikely, because NPM1 also has acidic tracts A1 and A2 in addition to a long acidic stretch of A3. It will be interesting to identify the domain within NPM3 that

interacts with the basic C-terminal domain of TP2. More importantly, we observed that acetylation of TP2 by p300 in its C-terminal domain completely abrogates its interaction with NPM3. We would like to believe that NPM3 being a member of the histone chaperone family may facilitate its assisted transport of TP2 from its entry to the nucleus until it is deposited on the spermatid chromatin. This putative chaperone function of NPM3 may be required to prevent any unnecessary interaction of the basic C-terminal domain of TP2 with nucleic acids *in vivo* before being deposited on to chromatin. Further experiments will be necessary in order to examine this hypothesis as well as the functional significance of the lack of interaction of acetylated TP2 with NPM3.

Acknowledgments—We thank Dr. Carol Parker at the UNC-Duke Proteomics Center for mass spectrometry analysis. We thank B. S. Suma and G. Roopa for help with confocal microscopy and MALDI-TOF analysis.

REFERENCES

1. Meistrich, M. L. (1989) in *Histones and Other Basic Nuclear Proteins* (Hnilica, L. S., Stein, G. S., and Stein, J. L., eds) pp. 165–182, CRC Press, Inc., Boca Raton, FL
2. Yu, Y. E., Zhang, Y., Unni, E., Shirley, C. R., Deng, J. M., Russell, L. D., Weil, M. M., Behringer, R. R., and Meistrich, M. L. (2000) *Proc. Natl. Acad. Sci. U.S.A.* **97,** 4683–4688
3. Wouters-Tyrou, D., Martinage, A., Chevaillier, P., and Sautière, P. (1998) *Biochimie* **80,** 117–128
4. Zhao, M., Shirley, C. R., Yu, Y. E., Mohapatra, B., Zhang, Y., Unni, E., Deng, J. M., Arango, N. A., Terry, N. H., Weil, M. M., Russell, L. D., Behringer, R. R., and Meistrich, M. L. (2001) *Mol. Cell. Biol.* **21,** 7243–7255
5. Zhao, M., Shirley, C. R., Mounsey, S., and Meistrich, M. L. (2004) *Biol. Reprod.* **71,** 1016–1025
6. Shirley, C. R., Hayashi, S., Mounsey, S., Yanagimachi, R., and Meistrich, M. L. (2004) *Biol. Reprod.* **71,** 1220–1229
7. Baskaran, R., and Rao, M. R. (1990) *J. Biol. Chem.* **265,** 21039–21047
8. Brewer, L., Corzett, M., and Balhorn, R. (2002) *J. Biol. Chem.* **277,** 38895–38900
9. Baskaran, R., and Rao, M. R. (1991) *Biochem. Biophys. Res. Commun.* **179,** 1491–1499
10. Kundu, T. K., and Rao, M. R. (1995) *Biochemistry* **34,** 5143–5150
11. Meetei, A. R., Ullas, K. S., and Rao, M. R. (2000) *J. Biol. Chem.* **275,** 38500–38507
12. Meetei, A. R., Ullas, K. S., Vasupradha, V., and Rao, M. R. (2002) *Biochemistry* **41,** 185–195
13. Ullas, K. S., and Rao, M. R. (2003) *J. Biol. Chem.* **278,** 52673–52680
14. Pradeepa, M. M., Manjunatha, S., Sathish, V., Agrawal, S., and Rao, M. R. (2008) *Mol. Cell. Biol.* **28,** 4331–4341
15. Roth, S. Y., Denu, J. M., and Allis, C. D. (2001) *Annu. Rev. Biochem.* **70,** 81–120
16. Sterner, D. E., and Berger, S. L. (2000) *Microbiol. Mol. Biol. Rev.* **64,** 435–459
17. Spange, S., Wagner, T., Heinzel, T., and Krämer, O. H. (2009) *Int. J. Biochem. Cell Biol.* **41,** 185–198
18. Christensen, M. E., Rattner, J. B., and Dixon, G. H. (1984) *Nucleic Acids Res.* **12,** 4575–4592
19. Hazzouri, M., Pivot-Pajot, C., Faure, A. K., Usson, Y., Pelletier, R., Sèle, B., Khochbin, S., and Rousseaux, S. (2000) *Eur. J. Cell Biol.* **79,** 950–960
20. Kundu, T. K., Wang, Z., and Roeder, R. G. (1999) *Mol. Cell. Biol.* **19,** 1605–1615
21. Yang, X., Ogryzko, V., Nishikawa, J., Howard, B., and Nakatani, Y. (1996) *Nature* **382,** 331–342
22. Kraus, W. L., and Kadonaga, J. T. (1998) *Genes Dev.* **12,** 331–342
23. Singh, J., and Rao, M. R. (1987) *J. Biol. Chem.* **262,** 734–740
24. Swaminathan, V., Kishore, A. H., Febitha, K. K., and Kundu, T. K. (2005) *Mol. Cell. Biol.* **25,** 7534–7545
25. Ullas, K. S., Pradeepa, M. M., Nikhil, G., Rammohan, N., and Rao, M. R. (2009) *J. Histochem. Cytochem.* **57,** 951–962
26. Steen, H., Pandey, A., Anderson, J. S., and Mann, M. (2002) *Sci. STKE 2002,* (154) PL16
27. Hansen, J. C., Ausio, J., Stanik, V. H., and Van Holde, K. E. (1989) *Biochemistry* **28,** 9129–9136
28. Kundu, T. K., and Rao, M. R. (1996) *Biochemistry* **35,** 15626–15632
29. Leuba, S. H., Yang, G., Robert, C., Samori, B., van Holde, K., Zlatanova, J., and Bustamante, C. (1994) *Proc. Natl. Acad. Sci. U.S.A.* **91,** 11621–11625
30. Allen, M. J., Bradbury, E. M., and Balhorn, R. (1997) *Nucleic Acids Res.* **25,** 2221–2226
31. Govin, J., Caron, C., Escoffier, E., Ferro, M., Kuhn, L., Rousseaux, S., Eddy, E. M., Garin, J., and Khochbin, S. (2006) *J. Biol. Chem.* **281,** 37888–37892
32. MacArthur, C. A., and Shackleford, G. M. (1997) *Genomics* **42,** 137–140
33. Marcon, L., and Boissonneault, G. (2004) *Biol. Reprod.* **70,** 910–918
34. Frehlick, L. J., Eirín-López, J. M., and Ausió, J. (2007) *BioEssays* **29,** 49–59
35. Huang, N., Negi, S., Szebeni, A., and Olson, M. O. (2005). *J. Biol. Chem.* **280,** 5496–5502
36. Zirwes, R. F., Schmidt-Zachmann, M. S., and Franke, W. W. (1997) *Proc. Natl. Acad. Sci. U.S.A.* **94,** 11387–11392
37. Motoi, N., Suzuki. K., Hirota, R., Johnson, P., Oofusa, K., Kikuchi, Y., and Yoshizato, K. (2008) *Dev. Growth Differ.* **50,** 307–320